Contents lists available at SciVerse ScienceDirect

Electrochimica Acta

Two-step sintering of ultrafine-grained barium cerate proton conducting ceramics

Siwei Wang [a], Lei Zhang [a], Lingling Zhang [a], Kyle Brinkman [b], Fanglin Chen [a,*]

[a] Department of Mechanical Engineering, University of South Carolina, Columbia, SC 29208, USA
[b] Savannah River National Laboratory, Aiken, SC 29808, USA

A B S T R A C T

Ultra-fine grained dense $BaZr_{0.1}Ce_{0.7}Y_{0.1}Yb_{0.1}O_{3-\delta}$ (BZCYYb) ceramics have been successfully prepared via a two-step sintering method. Co-precipitation method has been adopted to prepare nano-sized BZCYYb precursors with an average particle size of 30 nm. By controlling the sintering profile, an average grain size of 184 nm was obtained for dense BZCYYb ceramics via the two-step sintering method, compared to 445 nm for the conventional sintered samples. The two-step sintered BZCYYb samples showed less impurity and an enhanced electrical conductivity compared with the conventional sintered ones. Further, the two-step sintering method was applied to fabricate anode supported solid oxide fuel cells (SOFCs) using BZCYYb as the electrolyte, resulting in dense ultrafine-grained electrolyte membranes and porous anode substrates with fine particles. Due to the reduced ohmic as well as polarization resistances, the maximum power output of the cells fabricated from the two-step sintering method reached 349 mW m^{-2} at 700 °C, significantly improved from 172 mW cm^{-2} for the conventional sintered cells, suggesting that two-step sintering method is very promising for optimizing the microstructure and thus enhancing the electrochemical performances for barium cerate based proton-conducting SOFCs.

1. Introduction

It is widely known that microstructure of the ceramics has significant impact on the performances. In many cases the mechanical and electrical properties can be readily modified just by altering the grain size distributions without changing the compositions of the ceramics [1–3]. Many parameters, such as particle sizes of the reactant materials, fabrication methods, and even the microstructure of the green bodies will affect the final microstructures of the sintered ceramics [4]. In addition, the choice of sintering profiles plays a crucial role to adjust the final microstructure, especially the grain size distributions and densities of the ceramics. To obtain refined microstructure for the ceramic samples, advanced techniques such as spark-plasma sintering and high temperature microwave sintering have been utilized by rapidly heating the samples to high temperatures to prevent or suppress grain growth [5,6]. However, these advanced techniques are usually not assessable or affordable to most researchers and sometimes may induce unwanted heterogeneities [7].

As a promising alternative to prepare fine microstructured dense ceramics, the recently developed two-step sintering method has been proved to be less costly and more efficient [8]. With

appropriate sintering profile, the two-step sintering can produce fully densified ceramics with grains constrained down to nanometer size. The mechanism for the two-step sintering method is to suppress the grain boundary migration of the ceramics which occurs at high temperature, while enabling the grain boundary diffusion which occurs at relatively low temperature [8]. The first-stage high temperature sintering step helps eliminate supercritical pores while the second-stage low temperature sintering step suppresses grain growth [4]. This two-step sintering method has been applied with great success in obtaining dense ceramics with unique fine microstructures, including Y_2O_3 and SiC with nanometer-sized grains [8,9], CeO_2 and cubic structured zirconia (8 mol% Y_2O_3 stabilized) with ultrafine grains [10,11], and the perovskite structured barium titanite compound with ultrafine grain size below 200 nm [12].

Barium cerate-based ceramics have been extensively investigated due to their high proton conductivity at intermediate temperatures which can be applied in proton conducting solid oxide fuel cells (SOFCs), steam electrolysers and hydrogen separation membranes [13]. However, very limited reports are available to study the influence of microstructure on the electrochemical properties for the barium cerate-based ceramics. In this study, $BaZr_{0.1}Ce_{0.7}Y_{0.1}Yb_{0.1}O_{3-\delta}$ (BZCYYb) has been chosen due to its high ionic conductivity and good chemical stability [14]. We have demonstrated for the first time that ultrafine grained dense BZCYYb ceramics can be achieved via a two-step sintering method and

* Corresponding author. Tel.: +1 803 777 4875; fax: +1 803 777 0106.
E-mail address: chenfa@cec.sc.edu (F. Chen).

further evaluated the effect of microstructure on the electrical properties. In addition, the two-step sintering method has been applied to co-sinter an anode–electrolyte bi-layer to fabricate proton conducting SOFCs with significantly improved cell output power density.

2. Experimental

2.1. Powder synthesis and sample preparation

Powder samples of doped barium cerates having the nominal composition of $BaZr_{0.1}Ce_{0.7}Y_{0.1}Yb_{0.1}O_{3-\delta}$ (BZCYYb) were synthesized by a co-precipitation method as reported previously [10]. $Ba(NO_3)_2$ (Alfa Aesar, 99.95%), $Ce(NO_3)_3 \cdot 6H_2O$ (Alfa Aesar, 99.5%), $ZrO(NO_3)_2 \cdot xH_2O$ (Alfa Aesar, 99.9%), $Y(NO_3)_3 \cdot 6H_2O$ (Alfa Aesar, 99.9%) and $Yb(NO_3)_3 \cdot xH_2O$ (Alfa Aesar, 99.9%) were used as starting materials and dissolved in deionized water and titrated to determine the concentration of the metal ions. Stoichiometric ratio of each metal ion was taken and mixed with deionized water as precursors and $(NH_4)_2CO_3$ (Fisher Scientific, 95%) was used as the mineralizer. The precursors were dripped into the mineralizer at a rate of $3 \, mL \, min^{-1}$ under stirring. The obtained ivory-colored co-precipitate was washed with de-ionized water and ethanol to obtain a pH value of 7 and then filtered and dried. The obtained raw powders were subsequently calcined at $1100 \, °C$ for 5 h in air. The calcined powder was then pulverized and mixed with 5 wt% polyvinyl alcohol (PVA) binder and pressed uniaxially into pellets under 600 MPa (13 mm in diameter and about 1 mm in thickness) for further sintering study.

2.2. Sintering study

The pressed pellets were sintered by a two-step sintering method in which the samples were heated at $5 \, °C \, min^{-1}$ to $600 \, °C$ and held for 2 h to remove the organic PVA bonder, followed by heating at a rate of $5 \, °C \, min^{-1}$ to a peak temperature at $1450 \, °C$ and held for 1 min to achieve an intermediate density, then cooled at $15 \, °C \, min^{-1}$ to $1300 \, °C$ and held for 20 h, during which the ceramic densification was achieved while grain growth was suppressed [8]. As comparison, some pressed pellets were sintered by a conventional sintering method in which the pellets were heated to $600 \, °C$ and held for 2 h, followed by heating to $1450 \, °C$ at a heating rate of $5 \, °C \, min^{-1}$ and held for 5 h. Some co-precipitate raw powders were also pressed directly into pellets and sintered through a reactive sintering method in which the pellets were heated to $600 \, °C$ and held for 2 h, followed by heating to $1450 \, °C$ at a heating rate of $5 \, °C \, min^{-1}$ and held for 5 h, where the decomposition of the co-precipitate to form perovskite phase and subsequent sintering of the perovskite powders took place consecutively. The sintered pellets are named as Two-step, Conv., Reactive for samples sintered via two-step sintering method, conventional sintering method, and reactive sintering method, respectively.

2.3. Sample characterization

Crystalline phases of the samples were recorded on a X-ray diffractometer (Rigaku, Japan) with graphite-monochromatized CuKα radiation ($\lambda = 1.5418 \, Å$) using a scan rate of $5° \, min^{-1}$ in a 2θ range from $20°$ to $80°$. The sintering behavior of the material was carried out on samples using the same sintering profiles described above by a NETZSCH DIL 402C pushrod dilatometer. The microstructure of the samples was examined by a field emission scanning electron microscopy (FESEM, Zeiss Ultra) and transmission electron microscopy (TEM, Hitachi H-800, 200 kV). The porosities of the sintered pellets were quantified by a mercury porosimetry (Autopore IV, Micromeritics) at pressures ranging

from 0.5 psi to 30,000 psi. For the conductivity measurements, both surfaces of the sintered pellets were polished and painted with platinum paste (Heraeus, CL11-5349) followed by baking at $950 \, °C$ for 30 min. Platinum wires were then attached to the surface of the platinum layer. Electrical conductivity was measured using A.C. impedance method with A.C. amplitude of 10 mV in the frequency range from 0.1 Hz to 8 MHz using a Zahner IM6 Electrochemical Workstation (ZAHNER-Electrik GmbH & Co., Kronach, Germany). The conductivity tests were measured in wet air and wet H_2 containing 3 vol% H_2O, obtained by flowing gases through a water bubbler at room temperature.

2.4. Fuel cell fabrication and evaluation

For the electrochemical property measurements, anode supported BZCYYb fuel cells were prepared. The anode substrates containing NiO (J.T. Baker, 99%), BZCYYb and graphite (Alfa Aesar, 99.8%) with weight ratio of 3:2:1 were fabricated by die pressing at 100 MPa, followed by adding BZCYYb powder to the anode substrates and co-pressing the BZCYYb electrolyte powder onto the substrates at 300 MPa to form anode–electrolyte bi-layers [15]. Two-step sintering method with the same sintering profile as the BZCYYb pellets was used to sinter the anode–electrolyte bi-layer. $Ba_{0.9}Co_{0.7}Fe_{0.2}Nb_{0.1}O_{3-\delta}$ (BCFN) cathode ink [16] was prepared by ball-milling BCFN powders with V-006 organic solvent (Heraeus Materials, Germany) and then pasted on the BZCYYb electrolyte surface of the sintered NiO-BZCYYb bi-layers, followed by firing at $1000 \, °C$ for 2 h to form single cells. The two-step sintered anode supported BZCYYb single cells with the configuration of Ni-BZCYYb|BZCYYb|BCFN were sealed on alumina tubes by a ceramic bond (Ceramabond™ 552, Aremco Products Inc.). Single cells were tested with hydrogen (3 vol% H_2O) as the fuel with a flow rate of $40 \, mL \, min^{-1}$ and ambient air as the oxidant. The cells were first stabilized at $750 \, °C$ to allow complete reduction of NiO to Ni. Cell current and voltage characteristics were evaluated by a Versa STAT3-400 electrochemical station in the temperature range of $600–750 \, °C$. AC impedance spectra were measured under open circuit conditions with A.C. amplitude of 10 mV in the frequency range from 0.1 Hz to 1 MHz. The cross-section images of the single cells after electrochemical tests were taken using a field emission scanning electron microscopy (FESEM, Zeiss Ultra). The conventional sintered anode supported BZCYYb single cells with the same configuration were also tested for comparison.
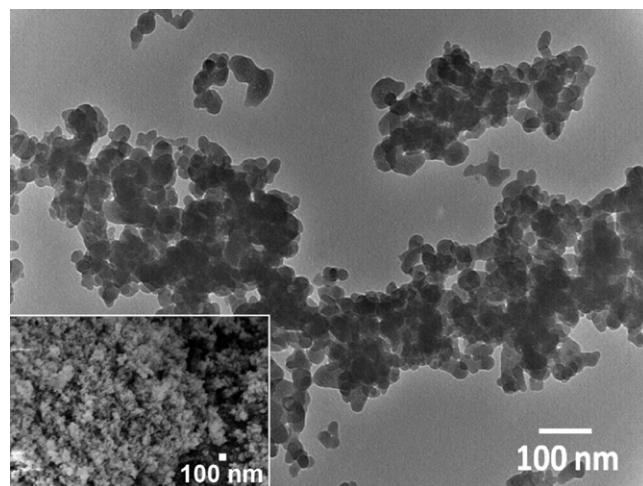

Fig. 1. TEM bright filed image of BZCYYb raw powder prepared by co-precipitation method. Inset is the FESEM picture of the powder.
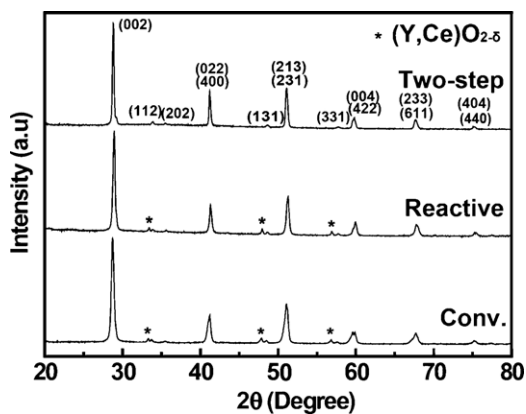
Fig. 2. XRD patterns of the sintered BZCYYb samples via conventional sintering method (Conv.), reactive sintering method (Reactive) and two-step sintering method (Two-step).

3. Results and discussion

3.1. Morphology and phase evolution

Fig. 1 shows the TEM bright field image of BZCYYb co-precipitated raw particles. Fig. 1 inset is the FESEM morphology of particles of the raw powder. It can be seen that fine particles with an average particle size around 30 nm are loosely agglomerated. The co-precipitation method adopted here produces spherical and uniform nano-sized grains, which is advantageous for the

decomposition to form BZCYYb phase and the subsequent densification of the BZCYYb ceramics.

Fig. 2 is the XRD patterns of the sintered pellets using different sintering methods. All the samples show predominantly orthorhombic perovskite structure similar to that of $BaCeO_3$ (JCPDS No. 22–0074). Since Y^{3+} (0.9 Å) and Yb^{3+} (0.868 Å) have similar ionic radii to that of Ce^{4+} (0.87 Å), a solid solution is expected to form by doping Y and Yb into Ce sites. Trace amount of $(Y, Ce)O_{2-\delta}$ impurity peaks was found in the conventional and reactive sintered samples. It was noted that there was $(Y, Ce)O_{2-\delta}$ impurity for both two-step sintered and conventional sintered samples after calcined at 1100 °C for 5 h. While after sintering, for the sample sintered via two-step sintering method, there was less impurity existed and thus was hard to discern by XRD. Based on the difference of the sintering profiles, the possible reason is that the $(Y, Ce)O_{2-\delta}$ dissolved into the lattice during the second holding stage for the two-step sintered samples. It is possible that $(Y, Ce)O_{2-\delta}$ diffuses and dissolves into the lattice with the grain boundary diffusion during the prolonged holding period at the second-stage with lower sintering temperature. The prolonged holding time is also beneficial for a higher solubility for the dopants and thus can be viewed as a homogenization process [17]. For conventional sintered and reactive sintered samples, the diffusion energy for the grain boundary is not met while the activation energy for grain boundary migration (grain growth) is guaranteed, leading to the segregation of the impurities in the grain boundaries. In addition, for conventional and reactive sintered samples, the possible Ba loss during high temperature sintering might also promote the formation of $(Y, Ce)O_{2-\delta}$ impurities [18,19].
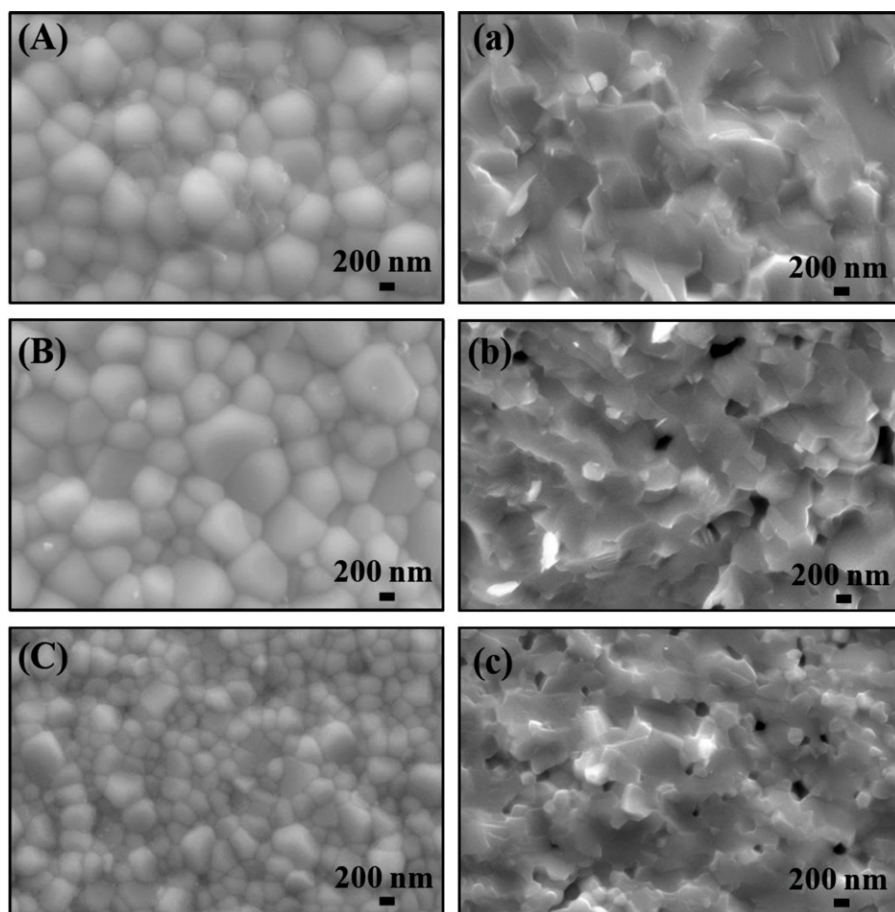

Fig. 3. FESEM pictures of BZCYYb sample pellets sintered via different profiles. Left: surface morphologies; right: cross-sectional morphology; (A, a) Conventional; (B, b) Reactive; (C, c) Two-step.
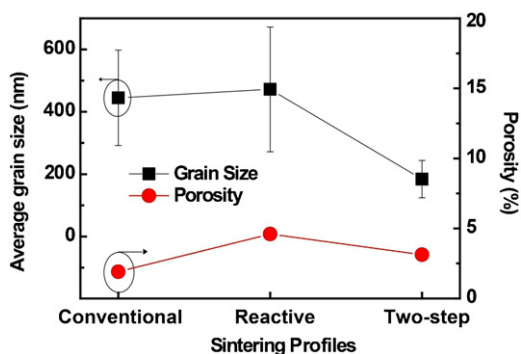
Fig. 4. Grain size and porosity distribution of BZCYYb ceramics with different sintering profiles.

Fig. 3(A)–(C) are the surface while Fig. 3(a)–(c) are the cross-sectional FESEM images of BZCYYb samples sintered via conventional sintering, reactive sintering, and two-step sintering, respectively. It can be seen that all the samples are well sintered with sub-micron grain sizes. Two-step sintered BZCYYb sample shows the finest grain size of 184 nm and a porosity of 3.13% measured by mercury porosimetry, compared with that of 445 nm with a porosity of 1.91% for conventional sintered sample. The difference in grain sizes is a clear indication that the activation energy for grain boundary migration is not satisfied while the grain boundary diffusion is active for BZCYYb by the two-step sintering profile. The detailed grain sizes and porosity distribution of the samples are shown in Fig. 4.

3.2. Sintering behaviors

The sintering behaviors of the samples were investigated by the dilatometry. Calcined samples were pressed into cylinders and sintered via two-step sintering and conventional sintering methods in the dilatometer. For reactive sintered samples, the raw powders were directly pressed into cylinders and measured by the dilatometer. Fig. 5 shows the dilatometric curves of BZCYYb samples with different sintering profiles. Inset is the expanded view of the linear shrinkage rate dL/dt. From the linear shrinkage curve dL/L_0 it can be seen that the sample from the reactive sintering method had the largest shrinkage during the sintering process. This is expected because in addition to the shrinkage at high temperature as a result of phase formation and densification process, considerable shrinkage took place at low temperature range (below 600 °C) due to removal of absorbed water and decomposition of the carbonates. Both the conventional sintering and two-step sintering methods showed similar trend up to 1450 °C since they have the same sintering profile prior to reaching 1450 °C. After the sample reached 1450 °C for 1 min, fast cooling rate helped
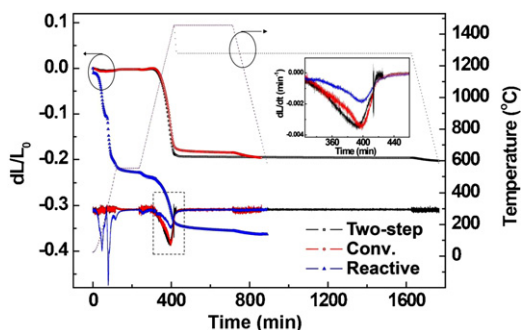

Fig. 5. Dilatometric curves of BZCYYb samples with different sintering profiles. Inset is the expanded view of the rate of change in linear shrinkage.
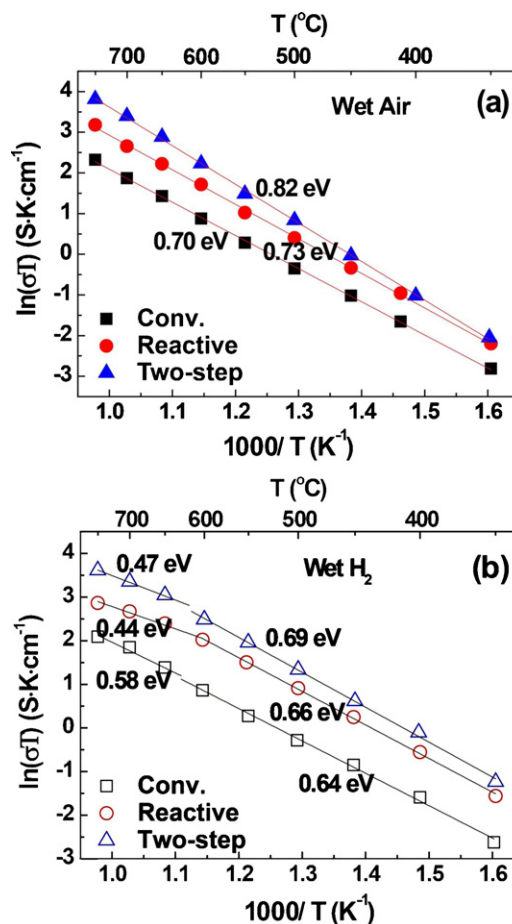

Fig. 6. Conductivity of BZCYYb samples measured in (a) wet air, and (b) wet H$_2$.

prevent additional grain growth, thus enabling further shrinkage for two-step sintered sample, consistent with modeling prediction that relatively fast cooling rate is preferred for two-step sintering method [7]. During this stage, the linear shrinkage percentage (dL/L_0) increased from 18.2% for the conventional sintered samples to 19.4% for the two-step sintered ones. From the linear shrinkage rate shown in the inset, the maximum shrinkage rate (dL/dt)$_{max}$ occurred around 398 min (at 1370 °C) for all the samples. A peak temperature of 1450 °C as the first sintering step is appropriate for the two-step sintered BZCYYb samples, since an intermediate density higher than 70% is necessary to guarantee the disappearance of supercritical pores while the other pores become subcritical and unstable against shrinkage to ensure a subsequent densified body at a lower holding temperature at 1300 °C [8].

3.3. Electrical conductivity

Fig. 6 presents the Arrhenius plot of the conductivity for BZCYYb in wet air and wet hydrogen, respectively. The activation energy can be calculated through the Arrhenius equation:

$$\sigma T = A \exp\left(-\frac{E_a}{RT}\right) \tag{1}$$

where A is the pre-exponential factor proportional to the charge carrier concentration, and E_a is the activation energy associated with the transport mechanism and can be calculated from the slopes in Fig. 6 [20]. The defect chemistry for proton conduction can be described as:
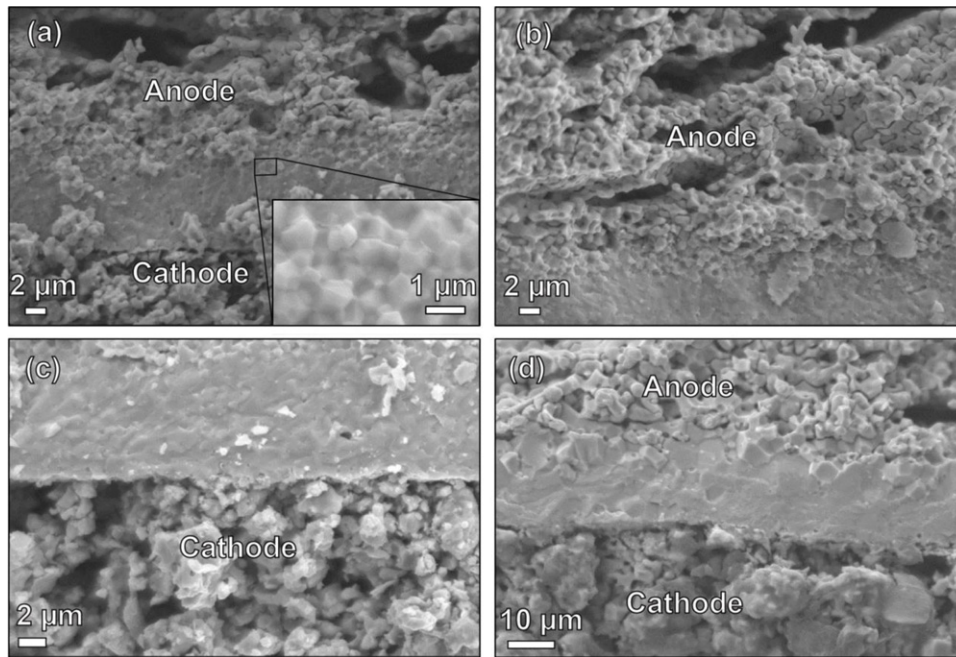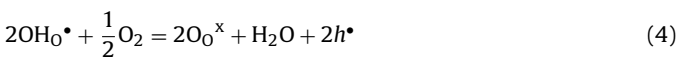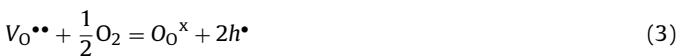
$$H_2O_{(g)} + O_O^x + V_O^{\bullet\bullet} = 2OH_O^\bullet \tag{2}$$

Fig. 7. Cross-sectional FESEM images of post-tested Ni-BZCYYb|BZCYYb|BCFN SOFC fabricated via two-step sintering method: (a) single cell, (b) anode–electrolyte interface, (c) cathode-electrolyte interface, and (d) single cell fabricated via conventional sintering method.

where $O_O{}^\times$ represents oxygen lattice, $V_O{}^{\bullet\bullet}$ denotes oxygen vacancy, and $OH_O{}^\bullet$ represents proton charge carrier formed within the structure by attaching to the oxygen lattice. It can be seen in Fig. 6 that for all the samples, the activation energy in wet air is higher than that in wet H_2, indicative of different conducting mechanisms. In wet air, the proton conductors are believed to be mixed conductions with the oxygen ion conduction competing with the proton conduction. The electronic hole conduction ($h^\bullet$) may also exist at high P_{O_2} and high temperatures via Eqs. (3) and (4):

$$V_O{}^{\bullet\bullet} + \frac{1}{2}O_2 = O_O{}^x + 2h^\bullet \tag{3}$$

$$2OH_O{}^\bullet + \frac{1}{2}O_2 = 2O_O{}^x + H_2O + 2h^\bullet \tag{4}$$

While in wet H_2, more protons tend to be active and mobile and are involved in the conduction process. There is also electronic conduction (e') at reduced atmospheres and high temperatures via Eq. (5):

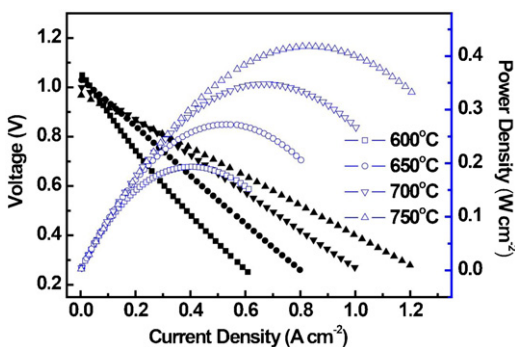$$\frac{1}{2}H_{2(g)} + O_O{}^x = OH_O{}^\bullet + e' \tag{5}$$

Fig. 8. Cell voltages and power densities as a function of current density for Ni-BZCYYb|BZCYYb|BCFN single cell via two-step sintering method.

The activation energies of proton and electronic conduction are smaller than those of oxygen ion and electronic hole conduction, leading to less gradient curves as shown in Fig. 6(b). In wet H_2, there is a decrease in the activation energy at high temperature regime (higher than 600 °C), which might be caused by the decrease in proton concentration due to the exothermal nature of proton defect formation in Eq. (2) [21]: the reaction tends to shift to the left side with increasing temperatures, resulting in a decreased proton concentration. Alternatively, it can be understood that water will evaporate at high temperatures, leading to a decrease in $OH_O{}^\bullet$ concentration. Although the proton mobility increases with temperature, the compensation effect leads to a decrease of the activation energy [22]. The activation energies of the BZCYYb samples prepared in this study show good agreement with those of samples prepared by glycine nitrate process [23], but are higher than those of samples prepared by solid state reaction method and modified Pechini method [14,24]. In general, activation energy can be influenced by several factors such as major charge carriers, phase transitions, or even sample degradation [25]. Different preparation methods may introduce different grain sizes and grain boundaries, and impurity levels in grain boundaries also play an important role to affect the activation energy [23]. In this study, conventional sintering, reactive sintering, and two-step sintering methods have been used to prepare the samples. Consequently, different grain sizes were shown for the samples from the different sintering methods. The impurity levels in grain boundaries were different as discussed previously, which would affect the concentrations of charge carriers, although competing effects may appear for the final activation energy value. In wet air atmosphere (Fig. 6(a)), the increased activation energy for two-step sintered samples is mainly due to the improved electronic hole conductivity in the grain boundary region (via Eqs. (3) and (4), where electronic hole conduction ($h^\bullet$) shows higher activation energy than that of proton conduction). While in wet H_2 atmosphere (Fig. 6(b)), at high temperatures (above 600 °C), the improved electronic conductivity in the grain boundary area (via Eq. (5), where electronic conduction (e') shows lower activation energy than that of proton conduction)
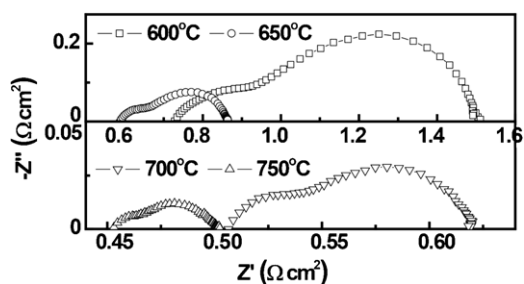
Fig. 9. Impedance spectra and resistances under open-circuit conditions of the single cell via two-step sintering method.

may lead to a lower activation energy for the two-step sintered sample.

In both air and H₂, the samples sintered by two-step sintering method show the highest conductivity, with 1.0×10^{-2} and 1.4×10^{-2} S cm^{-1} at 600 °C in wet air and wet H₂, respectively, followed by samples sintered via the reactive sintering method, while the samples sintered using the conventional sintering method have the lowest conductivity at the same testing conditions. The reason for the increase in conductivity may be attributed to the grain size effect on conductivity, and largely attributed to the improved grain boundary conductivity as a result from fewer amounts of impurity defects in the grain boundaries. The intrinsic grain boundary resistance may also play an important role to influence the grain boundary conductivity based on the space–charge model reported elsewhere [26,27]. It is noted the sample sintered by two-step sintering method shows similar conductivity compared with literature results [24], while the conventional sintered samples using powders prepared by a co-precipitation method exhibits lower conductivity compared with samples prepared by solid state reaction method and Pechini method [14,24], probably because of the secondary phases segregated in the grain boundaries which will deteriorate grain boundary conductivity and thus the total conductivity as reported in our previous study [24].

3.4. Microstructures of the fuel cells

The cross-sectional images of the single cell fabricated by two-step sintering method after electrochemical measurements are presented in Fig. 7(a)–(c). As a comparison, Fig 7(d) shows the cross-sectional image of a single cell via conventional sintering method. For both methods, the electrodes are well adhered to the electrolyte membranes. As shown in Fig. 7(a), for the cells fabricated by the two-step sintering method, the electrolyte is around 15 μm thick, with average grain sizes of 0.5 μm, compared to grains larger than 5 μm for the electrolyte sintered via conventional sintering method. The anode particles shown in Fig. 7(b) are also much smaller than those via the conventional sintering method (shown in Fig. 7(d) anode), advantageous to increase the triple-phase boundary (TPB) sites in the anode, where the electrochemical reaction occurs to produce protons [28].

3.5. Single cell performances

Fig. 8 shows the I–V curves and power densities of the BZCYYb cell fabricated by two-step sintering method. Maximum power densities of 193, 273, 349, and 418 mW cm^{-2} with the open circuit voltage (OCV) values of 1.05, 1.03, 1.0 and 0.97 V were obtained at 600, 650, 700 and 750 °C, respectively. The OCV values are consistent with the reported data indicative of the formation of sufficiently dense and gas tight electrolyte membrane [14,29]. Fig. 9 shows the impedance spectra of the cell measured under open circuit conditions. The ohmic resistance (R_o) of the cell was

Table 1
The ohmic resistance R_o, polarization resistance R_p, total resistance R_t, and their ratios obtained from the impedance spectra for Ni-BZCYYb|BZCYYb|BCFN single cell by two-step sintering method.

Temperature (°C)	R_o (Ω cm²)	R_p (Ω cm²)	R_t (Ω cm²)	R_o/R_t	R_p/R_t
600	0.73	0.76	1.49	49.0%	51.0%
650	0.59	0.27	0.86	68.6%	31.4%
700	0.51	0.11	0.62	82.3%	17.7%
750	0.45	0.05	0.50	90.0%	10.0%

determined from the intercept of the spectra with the real axis at high frequency while the total cell resistance (R_t) was determined by the intercept at low frequency. The polarization resistance (R_p) was determined by subtraction of the cell ohmic resistance from the total cell resistance. The R_o, R_p and R_t values and their ratios are presented in Table 1. The increase of the measuring temperature resulted in a significant reduction in both R_o and R_p. From R_o/R_t and R_p/R_t it can be seen that at temperatures higher than 700 °C the performance is strongly affected by the ohmic resistance, while at lower temperatures (such as 600 °C) the cell performance is limited by both ohmic and polarization resistances.

Fig. 10(a) shows the cell voltages and power outputs for BZCYYb samples sintered via two-step sintering and conventional sintering methods at 700 °C. Cell impedance spectra under open-circuit conditions are shown in Fig. 10(b). The open circuit voltages are about 1.0 V for both samples, indicating that by applying the two-step sintering method, the electrolyte membrane was as dense as that prepared by conventional sintering method. The maximum cell power output for BZCYYb sample sintered via two-step sintering is 177 mW cm^{-2} higher than that by conventional sintering method. The conductivities of the electrolyte films under fuel cell operation conditions were calculated to eliminate the difference of electrolyte thickness. Assuming that the ohmic resistance is caused solely by the electrolyte resistance, the BZCYYb electrolyte membrane in the cell prepared by two-step sintering method exhibited a conductivity of 0.0029 S cm^{-1}, compared with 0.0022 S cm^{-1} for the membrane in the cell prepared via conventional sintering. The conductivity is not directly comparable with that obtained in the conductivity measurement since the contact resistances between the electrode and the electrolyte were neglected. However, it suggests that enhanced electrolyte conductivity can be achieved via the two-step sintering in fuel cell conditions, which is consistent
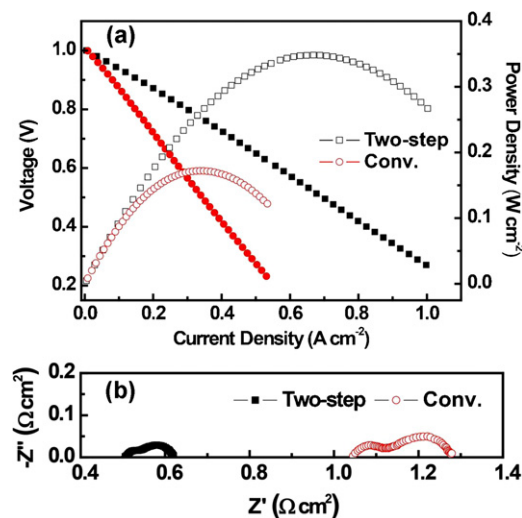

Fig. 10. (a) Comparison of cell voltage and power density at 700 °C for Ni-BZCYYb|BZCYYb|BCFN single cell via two-step sintering method (Two-step) and conventional sintering method (Conv.); (b) comparison of impedance spectra and resistances of the single cell under open-circuit conditions.

with the conductivity results. The polarization resistance for the two-step sintered fuel cell is also lower than that of conventional prepared fuel cell as shown in Fig. 10(b), which is mainly caused by the high porosity and ultrafine grain sizes for the anode to increase the TPB due to the low co-sintering temperature of the anode–electrolyte bi-layer. Overall, the two-step sintering method is a simple and effective way to fabricate Ni-based anode-supported proton conducting BZCYYb fuel cells with enhanced electrochemical performances.

4. Conclusions

Two-step sintering method was examined on BZCYYb proton conducting ceramics and ultrafine grained dense BZCYYb proton conductor was successfully prepared with a holding temperature of 1300 °C for 20 h. Compared with conventional sintering methods, higher sinterbility was observed from the dilatometric study for samples sintered by two-step sintering method. Increased conductivity, as well as lower ohmic resistance and enhanced cell power output was obtained for anode supported SOFCs using BZCYYb as the electrolyte in which the anode and electrolyte bi-layers were fabricated from two-step sintering method. All of these improvements indicate two-step sintering method is very promising to prepare barium cerate based dense proton-conducting ceramics and their anode supported SOFCs.

Acknowledgement

References

[1] Y.M. Chiang, E.B. Lavik, I. Kosacki, H.L. Tuller, J.Y. Ying, Applied Physics Letters 69 (1996) 185.
[2] M.H. Fathi, M. Kharaziha, Materials Letters 63 (2009) 1455.
[3] W. Puin, S. Rodewald, R. Ramlau, P. Heitjans, J. Maier, Solid State Ionics 131 (2000) 159.
[4] K. Maca, V. Pouchly, P. Zalud, Journal of the European Ceramic Society 30 (2010) 583.
[5] L. An, A. Ito, T. Goto, Journal of the American Ceramic Society 94 (2011) 695.
[6] K.H. Brosnan, G.L. Messing, D.K. Agrawal, Journal of the American Ceramic Society 86 (2003) 1307.
[7] M.A. Lourenço, G.G. Cunto, F.M. Figueiredo, J.R. Frade, Materials Chemistry and Physics 126 (2011) 262.
[8] I.-W. Chen, X.-H. Wang, Nature 404 (2000) 168.
[9] Y.-I. Lee, Y.-W. Kim, M. Mitomo, D.-Y. Kim, Journal of the American Ceramic Society 86 (2003) 1803.
[10] L. Zhang, F. Chen, C. Xia, International Journal of Hydrogen Energy 35 (2010) 13262.
[11] M. Mazaheri, Z.R. Hesabi, F. Golestani-Fard, S. Mollazadeh, S. Jafari, S.K. Sadrnezhaad, Journal of the American Ceramic Society 92 (2009) 990.
[12] Z. Tian, X. Wang, S. Lee, K.H. Hur, L. Li, Journal of the American Ceramic Society 94 (2011) 1119.
[13] H. Iwahara, Solid State Ionics 28 (1988) 573.
[14] L. Yang, S.Z. Wang, K. Blinn, M.F. Liu, Z. Liu, Z. Cheng, M.L. Liu, Science 326 (2009) 126.
[15] F. Zhao, S. Wang, L. Dixon, F. Chen, Journal of Power Sources 196 (2011) 7500.
[16] Z. Yang, C. Yang, C. Jin, M. Han, F. Chen, Electrochemistry Communications 13 (2011) 882.
[17] C.-W. Nahm, Materials Letters 58 (2004) 3297.
[18] J. Lv, L. Wang, D. Lei, H. Guo, R.V. Kumar, Journal of Alloys and Compound 467 (2009) 376.
[19] Y. Guo, R. Ran, Z. Shao, International Journal of Hydrogen Energy 35 (2010) 5611.
[20] R. Pflieger, M. Malki, Y. Guari, J. Larionova, A. Grandjean, Journal of the American Ceramic Society 92 (2009) 1560.
[21] K.D. Kreuer, Annual Review of Materials Research 33 (2003) 333.
[22] Z. Sun, E. Fabbri, L. Bi, E. Traversa, Journal of the American Ceramic Society 95 (2012) 627.
[23] X. Zhou, L. Liu, J. Zhen, S. Zhu, B. Li, K. Sun, P. Wang, Journal of Power Sources 196 (2011) 5000.
[24] S. Wang, F. Zhao, L. Zhang, F. Chen, Solid State Ionics 213 (2012) 29.
[25] E. Fabbri, I. Markus, L. Bi, D. Pergolesi, E. Traversa, Solid State Ionics 202 (2011) 30.
[26] C. Kjølseth, H. Fjeld, Ø. Prytz, P.I. Dahl, C. Estournès, R. Haugsrud, T. Norby, Solid State Ionics 181 (2010) 268.
[27] C.M. Fernandes, A. Castela, F.M. Figueiredo, J.R. Frade, Solid State Ionics 193 (2011) 52.
[28] Q. Liu, X. Dong, C. Yang, S. Ma, F. Chen, Journal of Power Sources 195 (2010) 1543.
[29] F. Zhao, C. Jin, C. Yang, S. Wang, F. Chen, Journal of Power Sources 196 (2011) 688.